CrossMark

# Synthesis of highly crystalline photocatalysts based on TiO$_2$ and ZnO for the degradation of organic impurities under visible-light irradiation

Adam Kubiak[1] · Katarzyna Siwińska-Ciesielczyk[1] · Zuzanna Bielan[2] · Anna Zielińska-Jurek[2] · Teofil Jesionowski[1]

## Abstract

A TiO$_2$–ZnO binary oxide system (with molar ratio TiO$_2$:ZnO = 8:2) was synthesized by a hydrothermal method, assisted by calcination at temperatures of 500, 600 and 700 °C, using zinc citrate as the precursor of ZnO. The morphology (SEM, TEM), crystalline structure (XRD, Raman spectroscopy), diffuse reflectance spectra (DRS), chemical surface composition (EDXRF), porous structure parameters (low-temperature N$_2$ sorption) and characteristic functional groups (FT-IR) of the TiO$_2$–ZnO oxide materials were comprehensively analyzed. The novelty of this work is the observation of the coexistence of the crystalline structures of anatase and ZnTiO$_3$ in TiO$_2$–ZnO oxide materials. Moreover, it is shown that the obtained materials absorb visible radiation. The key stage of the study was the evaluation of the photocatalytic activity of the TiO$_2$–ZnO binary oxide systems in the degradation of model organic pollutants: C.I. Basic Red 1, C.I. Basic Violet 10, C.I. Basic Blue 3 and 4-nitrophenol. For all synthesized materials, a high efficiency of degradation of the model organic impurities was demonstrated. The results show that the synthesized products may be materials of interest for use in the degradation of organic pollutants. Moreover, the kinetics of the photocatalytic degradation of selected organic compounds were determined based on the Langmuir–Hinshelwood equation, assuming a pseudo-first-order (PFO) reaction.
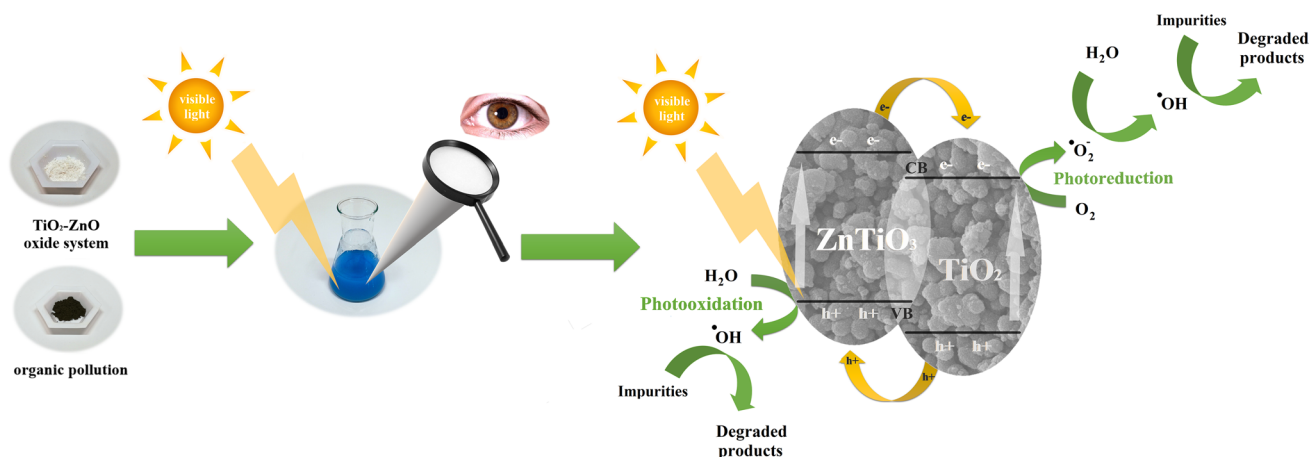
**Keywords** Titania · Zinc oxide · Binary oxide systems · Hydrothermal synthesis · Photocatalysis

# 1 Introduction

Much attention has been paid in recent years to the discharge of sewage containing toxic organic pollutants such as synthetic dyes and phenol derivatives. Synthetic dyes are very common pollutants: globally 280,000 tons of dyes are

✉ Teofil Jesionowski
teofil.jesionowski@put.poznan.pl

Extended author information available on the last page of the article

discharged in industrial effluents every year (Jin et al. 2007; Miranda et al. 2013). For example, the coloring of 1 kg of cotton with reactive dyes requires 0.6–0.8 kg of NaCl, 30–60 g of dyestuff and 70–150 dm³ of water. The resulting wastewater contains 20–30% of the toxic pollutants, with an average concentration of 2000 ppm of organic dye (Esparza et al. 2007). Synthetic dyes are produced and consumed in large quantities, and can cause considerable environmental pollution and serious health risks due to their stability and toxicity (Shukla and Gupta 1992). To reduce the negative impact on the environment, many methods of removing dyes from water and wastewater have been developed; however, conventional water treatment technologies such as solvent extraction and chemical treatment processes often produce hazardous by-products and generate large amounts of solid wastes, which is not environmentally friendly (Galindo et al. 2001; Pandurangan et al. 2001; Slokar and Le Marechal 1998).

Another group of very dangerous organic pollutants is phenol derivatives. Nitrophenols are among the most resistant compounds, being highly stable and soluble in water (Gandhi et al. 2012; Kang et al. 2009; Peretz and Cinteza 2008). 4-Nitrophenol and its derivatives are obtained in the production of pesticides and herbicides (Parida and Das 2004). This compound is used as an indicator, as a chemical intermediate for the insecticide methyl parathion, for the production of azo and sulfur dyes, and for other purposes (Peretz and Cinteza 2008).It is considered a very dangerous pollutant, and is classed as a priority toxic pollutant by the U.S. Environmental Protection Agency. The maximum allowed concentration in water is in the range 1–20 ppb (Chen and Ray 1998; Mishra and Gogate 2011; Peretz and Cinteza 2008).

The current scientific literature indicates the wide use of many techniques for the treatment of wastewater against common pollutants. They include membrane techniques (Szczygielda and Prochaska 2018), adsorption (Bartczak et al. 2015), biocatalysis (Antecka et al. 2018) and photocatalysis (Rahim Pouran et al. 2015, 2016, 2018a, b). Methods such as membrane techniques or biocatalysis are classed as high-cost processes. They give satisfactory results; however, creating a membrane or biocatalyst is expensive. Furthermore, attention has to be paid to the narrow limits of membrane or biocatalyst strength (parameters limiting the pressure or temperature). Therefore, the process of photocatalysis with the use of popular oxides with semiconductor properties such as $TiO_2$ (Kubiak et al. 2018), ZnO (Kolodziejczak-Radzimska and Jesionowski 2014) or CuO (Zhang et al. 2014) seems to be particularly interesting. The most popular photocatalyst among commonly available materials is titanium dioxide (Konstantinou and Albanis 2004; Kuvarega and Mamba 2017; Li et al. 2015; Nakata and Fujishima 2012). It is characterized by a wide

band gap of 3.2 eV (Henderson 2011). However, its greatest disadvantage is that UV light is required for the photocatalytic oxidation process (Chen and Burda 2008; Cong et al. 2007; Kumar and Devi 2011). Because solar radiation contains only 3–5% UV radiation, this hinders the use of materials such as $TiO_2$ in industrial photocatalytic processes (Siwińska-Stefańska et al. 2018). To improve the properties of titanium dioxide, it may be modified (Delsouz Khaki et al. 2018a, b; Khaki et al. 2017). Many studies have shown that the addition of ZnO causes a significant improvement in the photocatalytic activity of $TiO_2$ (Delsouz Khaki et al. 2018a, b). Furthermore, in these materials, the formation of zinc titanate ($ZnTiO_3$) is observed; this compound exhibits activity in visible light (Kong et al. 2009; Perween and Ranjan 2017; Yan et al. 2015), which is desirable in the industrial application of this type of material.

In this work, zinc citrate was used for the first time as a precursor of ZnO in the synthesis of $TiO_2$–ZnO oxide systems, using a hydrothermal method assisted by calcination. The hydrothermal method has been indicated as interesting for the synthesis of this type of materials due to the possibility of obtaining a specific crystal structure and designed morphology. In addition, the small number of literature reports regarding the synthesis of this type of materials using hydrothermal treatment should be noted. Moreover, to determine changes in the crystal structure, the synthesized $TiO_2$–ZnO oxide system was additionally subjected to calcination at temperatures of 500, 600 and 700 °C. It was investigated how the temperature of calcination affects the morphology and the crystalline and porous structure of the products. The key stage of the research was the evaluation of the photocatalytic activity of the synthesized oxide materials in the degradation of model organic pollutants: C.I. Basic Blue 3, C.I. Basic Red 1, C.I. Basic Violet 10 and 4-nitrophenol. Additionally, the kinetics of the photooxidation process were investigated using the Langmuir–Hinshelwood equation, assuming that the decomposition of the pollutants follows a pseudo-first-order (PFO) reaction.

## 2 Experimental

### 2.1 Materials

Titanium(IV) isopropoxide (TTIP, 97%), zinc citrate dihydrate (97%), C.I. Basic Blue 3 (BB3, 25%), C.I. Basic Red 1 (BR1, 95%), C.I. Basic Violet 10 (BV10, 97%) and 4-nitrophenol (4-NF, 99%) were purchased from Sigma-Aldrich (USA). Propan-2-ol (IPA, 99.5%) and solution of ammonium hydroxide (10%) were purchased from Chempur (Poland). All reagents were of analytical grade and used without any further purification. The water used in all experiments was deionized.

## 2.2 Preparation of TiO₂–ZnO oxide systems

In the first stage of the synthesis, to a reactor equipped with a high-speed stirrer (Eurostar Digital, Ika Werke, Germany), 25 cm³ of the solvent (propan-2-ol) and an appropriate amount of titanium(IV) isopropoxide (TTIP) were added. In this study, the materials were obtained at the molar ratio $TiO_2{:}ZnO = 8{:}2$. We also investigated other molar ratios; however, the products proved to be inferior to the materials described, and are therefore omitted from this work. To produce $TiO_2$–ZnO binary oxide systems, 15% zinc citrate solution (15 g of zinc citrate dissolved in 100 cm³ of 10% ammonium hydroxide) was added to the mixture of TTIP and IPA at a predetermined rate (5 cm³/min) using an ISM833A peristaltic pump (ISMATEC, Germany). The reaction system was stirred at a predetermined speed of 1000 rpm for 1 h. The resulting mixture (100 cm³) was transferred to an autoclave and subjected to hydrothermal treatment at 200 °C for 24 h. The hydrothermal reactor was cooled at room temperature, and the resulting material was filtered and washed three times with deionized water. The $TiO_2$–ZnO powder was then dried at 60 °C for 6 h. In the last step, the material was calcined at a temperature of 500, 600 or 700 °C for 2 h in atmospheric air (Nabertherm P320 Controller, Germany). These calcination temperatures were selected to improve the physicochemical properties of the synthesized binary oxide systems, such as the crystalline structure. All of the synthesized materials were subjected to classification. The obtained $TiO_2$–ZnO oxide systems were labeled as TiZn (material subjected to hydrothermal treatment only), TiZn_500 (calcined at 500 °C), TiZn_600 (calcined at 600 °C) and TiZn_700 (calcined at 700 °C).

## 2.3 Characterization of synthesized materials

The morphology and microstructure of the samples were examined using scanning and transmission electron microscopy (SEM and TEM). The SEM images were taken with an EVO40 instrument (Zeiss, Germany). The TEM analysis was carried out using a Jeol 1200 EX II apparatus (Jeol, USA) at an accelerating voltage of 100 kV.

X-ray diffraction (XRD) analysis was used to determine the crystalline structure of the materials. The XRD analysis was performed using a D8 Advance X-ray diffractometer (Bruker, Germany) with Cu 40 Kα, 30 mA and Ni filter. The patterns were obtained in step-scanning mode ($\Delta 2\theta = 0.05°$) over an angular range of 20°–80°. In addition, Raman spectroscopy was performed using a Bruker Bravo analyzer (Bruker, Germany), equipped with two lasers covering a wavelength range of 700–1100 nm. To obtain the Raman spectrum, the tested material was applied to a glass slide and placed in a measuring cell. Raman shifts were measured in the range 800–300 cm⁻¹.

To evaluate the light-absorption properties of the $TiO_2$–ZnO photocatalysts, diffuse reflectance spectra (DRS) were recorded. The data were converted to obtain the absorption spectra. The band gap energies of the photocatalysts were calculated from the corresponding Kubelka–Munk function, $F(R) = (1 - R)^2/2R$, where R is reflectance, which is proportional to the absorption of radiation, by plotting $F(R)^{0.5}E_{ph}^{0.5}$ against $E_{ph}$, where $E_{ph}$ is photon energy. The measurements were carried out using a Thermo Scientific Evolution 220 (Waltham, USA) spectrophotometer with a PIN-757 integrating sphere.

The surface composition of the $TiO_2$–ZnO oxide systems was determined using an Epsilon1 EDXRF spectrometer (PANalytical, United Kingdom), operating based on energy dispersion (EDXRF). The spectrometer is equipped with an X-ray tube with an Ag 5 W anode and a 50 kV generator with 500 µA current, a set of six measurement filters and a high-resolution SDD semiconductor detector cooled by the Peltier effect.
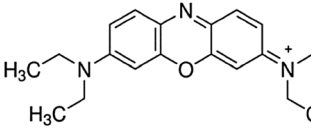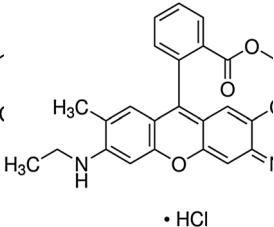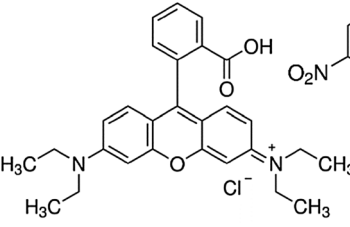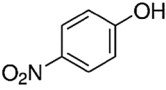
Porous structure parameters (BET surface area, pore volume and pore diameter) were determined using an ASAP 2020 physisorption analyzer (Micromeritics Instrument Co., USA) by the Brunauer–Emmett–Teller (BET) method based on low-temperature $N_2$ sorption. Before measurement, the materials were degassed at 120 °C for 4 h. The surface area was determined by the multipoint BET method using adsorption data in a relative pressure ($p/p_0$) range of 0.05–0.30.

Fourier transform infrared spectroscopy was performed using a Vertex 70 instrument (Bruker, Germany). The samples were analyzed in the form of tablets, made by pressing a mixture of anhydrous KBr (ca. 0.1 g) and 1 mg of the tested sample in a special steel ring, under a pressure of approximately 10 MPa. The analysis was performed over a wavenumber range of 4000–400 cm⁻¹.

## 2.4 Photocatalytic tests

The photocatalytic activity of the obtained $TiO_2$–ZnO binary oxide systems was evaluated based on the decomposition of selected impurities: C.I. Basic Blue 3 (BB3), C.I. Basic Red 1 (BR1), C.I. Basic Violet 10 (BV10) and 4-nitrophenol (4NF) (see Table 1), with an initial concentration of 10 mg/dm³. Photocatalytic activity was determined using a laboratory reactorof UV-RS2 type (Heraeus, Germany), equipped with a 150 W medium-pressure mercury lamp as a visible light source, surrounded by a water-cooling glass jacket. To assess the degradation in visible light, a glass lamp with a water jacket that excluded UV radiation was used. In the first step, 0.8 g/dm³ of photocatalyst (TiZn, TiZn_500, TiZn_600 or TiZn_700) was added to a glass tube reactor containing 100 cm³ of the model organic impurity. The suspension was stirred using an R05 IKAMAG magnetic stirrer (IKA Werke

**Table 1** Basic data of organic impurities used in photocatalytic tests

| Color Index Name | C.I. Basic Blue 3 | C.I. Basic Red 1 | C.I. Basic Violet 10 | 4-nitrophenol |
| --- | --- | --- | --- | --- |
| Chemical structure | | | | |
| Molecular formula | $C_{16}H_{18}ClN_3S \cdot 3H_2O$ | $C_{28}H_{31}ClN_2O_3$ | $C_{28}H_{31}ClN_2O_3$ | $C_6H_5NO_3$ |
| Molar mass (g/mol) | 373.85 | 479.01 | 479.01 | 139.11 |
| $\lambda_{max}$ (nm) | 654 | 526 | 553 | 400 |

GmbH, Germany) for 30 min in darkness, to determine the adsorption/desorption equilibrium. After this time, the radiation was turned on to initiate the photocatalytic reaction. The process was carried out for a maximum of 360 min in order to obtain a plateau. However, a very high efficiency of photodegradation was obtained after 180 min. The irradiated mixtures were collected from the reactor at regular intervals (30 min) and centrifuged to separate the photocatalyst. The concentration of C.I. Basic Blue 3, C.I. Basic Red 1, C.I. Basic Violet 10 and 4-nitrophenol (after adsorption and Vis-irradiation) was analyzed using a UV–Vis spectrophotometer (V-750, Jasco, Japan) at a wavelength of 654 nm for BB3, 526 nm for BR1, 553 nm for BV10 and 400 nm for 4-NF, using water as a reference. The photocatalytic activity of the obtained materials was determined by calculating the yield of impurity degradation (W), using the formula:

$$W(\%) = \left(1 - \frac{C_t}{C_0}\right) \times 100\%, \tag{1}$$

where $C_0$ and $C_t$ are the concentrations of the impurity prior to and after irradiation respectively.

## 2.5 Kinetic study of photocatalysis

A significant number of researchers working on heterogeneous photocatalysis have reported that the kinetics of the photooxidation of various impurities in the presence of $TiO_2$ photocatalysts follow the Langmuir–Hinshelwood kinetic model:

$$r = \frac{dC}{dt} = k\left(\frac{KC}{1 + KC}\right) \tag{2}$$

In the present study we assumed that the decomposition of the pollutants takes place in a pseudo-first-order reaction, so that the constant rate of reaction can be determined as the slope of the linear regression. Therefore, the equation presents the dependence between the impurity concentration

in the aqueous phase and the time of UV irradiation, and can be written as follows:

$$-\ln\left(\frac{C_t}{C_0}\right) = kt \tag{3}$$

where $k$ is the rate of degradation of the organic pollutant (1/min), $K$ is the equilibrium constant of adsorption of the pollutant on the surface of the catalyst, and $C_0$, $C_t$ are the concentrations of the pollutant in aqueous solution before irradiation ($t = 0$) and after a defined irradiation time $t$.

Knowledge of the constant reaction rate $k$ allows one to determine the half-life of the model organic pollutants, based on the equation:

$$t_{\frac{1}{2}} = \frac{\ln 2}{k} \tag{4}$$

## 3 Results and discussion

### 3.1 Characteristics of the synthesized photocatalysts

The first stage of physicochemical analysis involved evaluation of the morphology and microstructure of the obtained photocatalysts. To determine the morphology, SEM and TEM analysis were performed. SEM images are shown in Fig. 1, and TEM images in Fig. 2.

All of the oxide materials obtained have a similar morphology. Both the hydrothermal (TiZn) and the calcined materials (TiZn_500, TiZn_600 and TiZn_700) contained agglomerated spherical particles. No single particles were observed in the SEM images. In addition, for all analyzed materials, the agglomerates were found to be smaller than 1 μm. The temperature of thermal treatment was not found to influence the morphology or microstructure of the $TiO_2$–ZnO oxide systems.

**Fig. 1** SEM images of TiO$_2$–ZnO oxide systems: **a** TiZn, **b** TiZn_500, **c** TiZn_600 and **d** TiZn_700
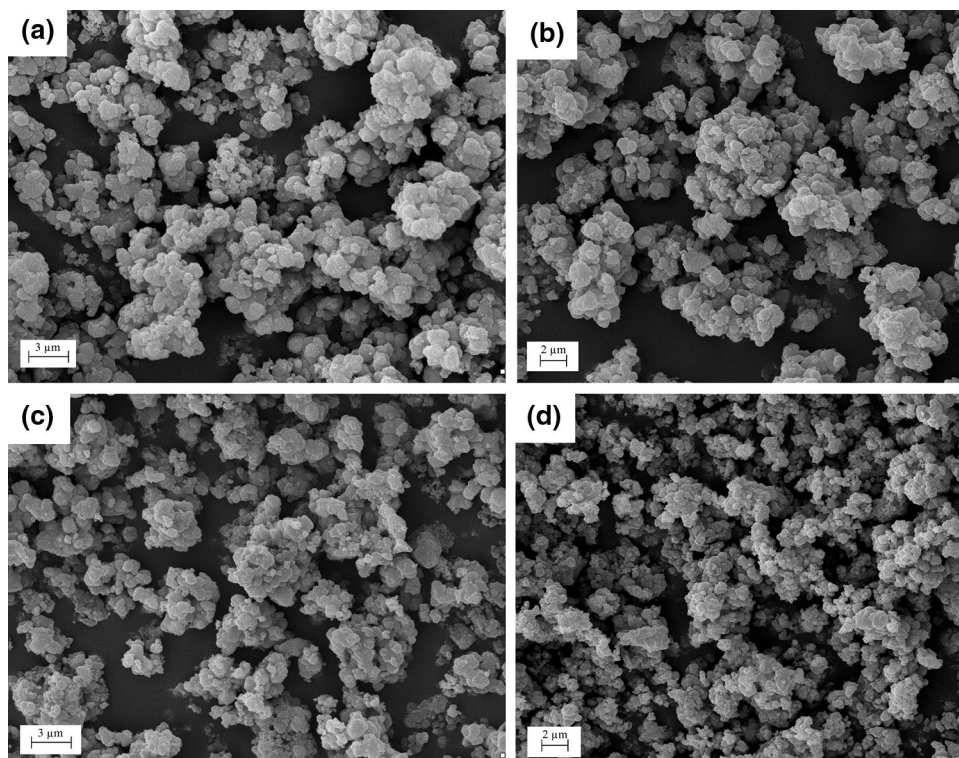


Morphology was further analyzed using TEM. The obtained TEM images are presented in Fig. 2.

Analysis of the TEM images shows that the samples TiZn (Fig. 2a) and TiZn_500 (Fig. 2b) have a similar morphology. These materials have particles of single nanometer size with a tendency to agglomerate. In addition, for the samples TiZn_600 (Fig. 2c) and TiZn_700 (Fig. 2d), sintering related to the calcination process is observed. For TiZn_600, individual particles were observed with a larger size than in the case of TiZn and TiZn_500. However, for TiZn_700 only large aggregates associated with the closure of the porous structure were observed. The morphological analysis showed that as the temperature of thermal treatment increased, the diameter of the particles shifted towards higher values, as a result of their sintering and greater agglomeration (Wang et al. 2015; Oghbaei and Mirzaee 2010; Roy et al. 1999).

Xu et al. (2011) used a hydrothermal method and a calcination process for the synthesis of TiO$_2$–ZnO oxide systems. The products contained spherical particles with a tendency towards agglomeration; however, the materials in that study had a smaller particle size. Pant et al. (2013) obtained TiO$_2$–ZnO binary oxide systems by a facile hydrothermal process. The materials produced contained spherical-like particles with a tendency to agglomerate. Fatimah and Novitasari (2016) synthesized a TiO$_2$–ZnO oxide system using the sol–gel method and a calcination process. The materials obtained with a molar ratio of TiO$_2$:ZnO = 5:1 contained irregularly shaped particles.

The results obtained from TEM analysis are consistent with the literature (Pérez-González et al. 2017; Vlazan et al. 2015). Vlazan et al. (2015) also obtained a TiO$_2$–ZnO oxide system via a hydrothermal method; the TEM images of the obtained powders showed individual particles of nanometric size (> 50 nm). The observed sintering effect produced by the calcination process is well described in the literature (Chen et al. 2015; Konyar et al. 2012; Luo and Zhang (2015); Nie et al. 2015). In the cited studies it was shown that the calcination process causes the disappearance of individual particles, and closure of the porous structure is observed.

In comparison with materials previously reported in the literature (Chang et al. 2004; Tian et al. 2017; Wu et al. 2016), the materials obtained in the present work have similar morphology, in particular the samples TiZn and TiZn_500, which contain spherical, nanometric size particles with a tendency to agglomerate. The materials TiZn_600 and TiZn_700 have a smaller particle size than similar materials described by other researchers. It was found that, as the calcination temperature increased, the particle diameter also increased.

At the next stage of physicochemical analysis, the crystalline structure parameters of the obtained photocatalysts were determined. These are among the most important properties, because they determine the possibility of using the synthesized material for specific applications. To describe the crystalline structure, both X-ray diffraction and Raman

**Fig. 2** TEM images of synthesized binary oxide materials: **a** TiZn, **b** TiZn_500, **c** TiZn_600 and **d** TiZn_700
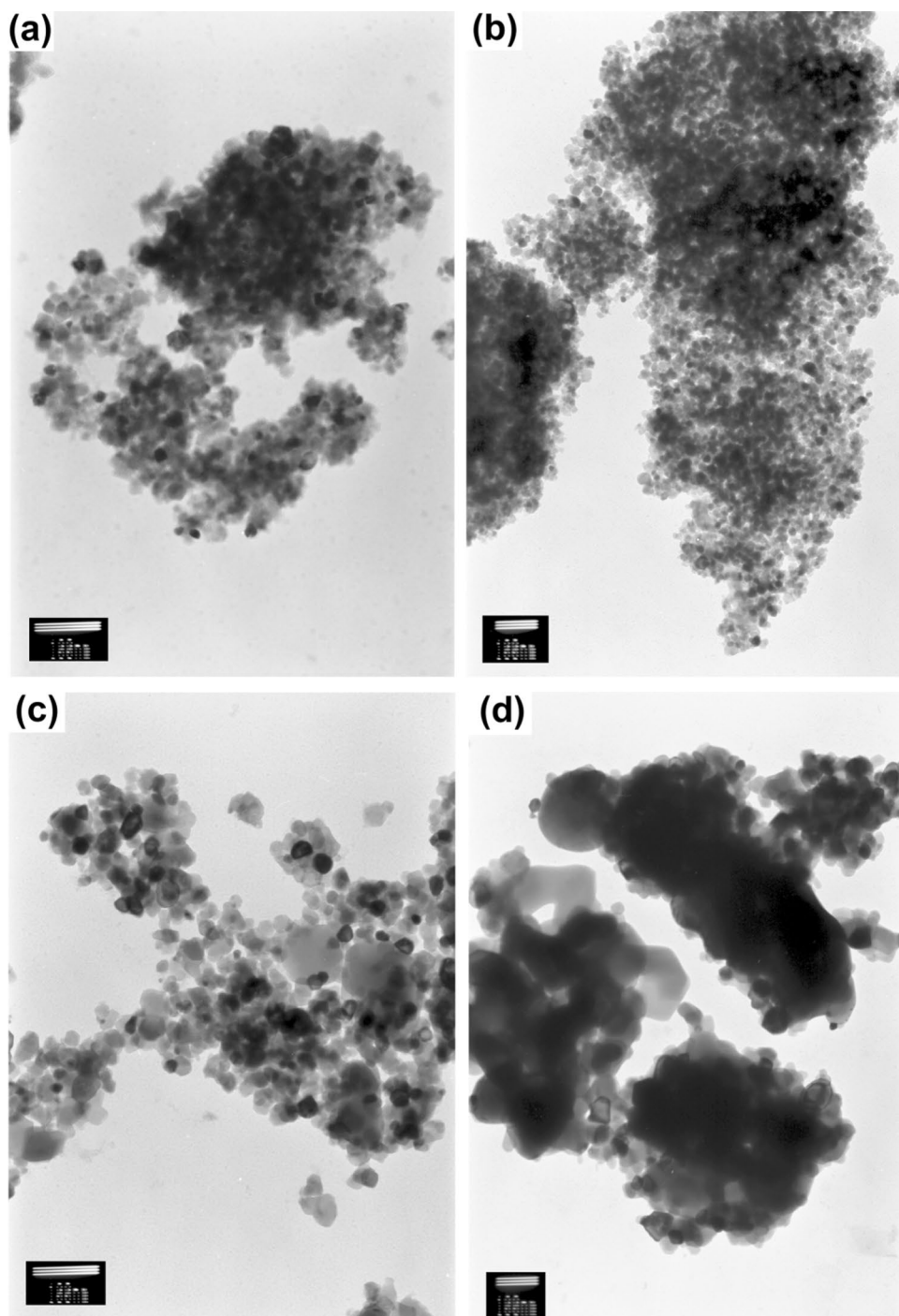
spectroscopy were applied. The XRD patterns and Raman spectra for the obtained materials are shown in Fig. 3.

The XRD pattern for sample TiZn showed that this material contains the crystalline structure of anatase (JCPDS No. 21-1272)—see Fig. 3a. Diffraction peaks were observed at 2θ values of 25.28, 37.8, 48.05, 53.81, 55.11, 62.69, 68.76, 70.31 and 76. For all of the $TiO_2$–ZnO oxide systems obtained in this work, the same diffraction bands characteristic of anatase were observed. The oxide system calcined at

500 °C (TiZn_500) has the crystalline structure of anatase and zinc titanate (JCPDS No. 14-0033). Diffraction reflections from anatase were observed, as well as peaks derived from zinc titanate ($ZnTiO_3$) at 32.71 and 35.21. A significant improvement in the crystalline structure is observed for the material TiZn_600. In this case, the formation of the $ZnTiO_3$ structure was shown to be improved compared with TiZn_500; characteristic peaks for this crystalline structure were observed at the 2θ values 21.1, 23.91, 32.7, 35.2, 40.4,
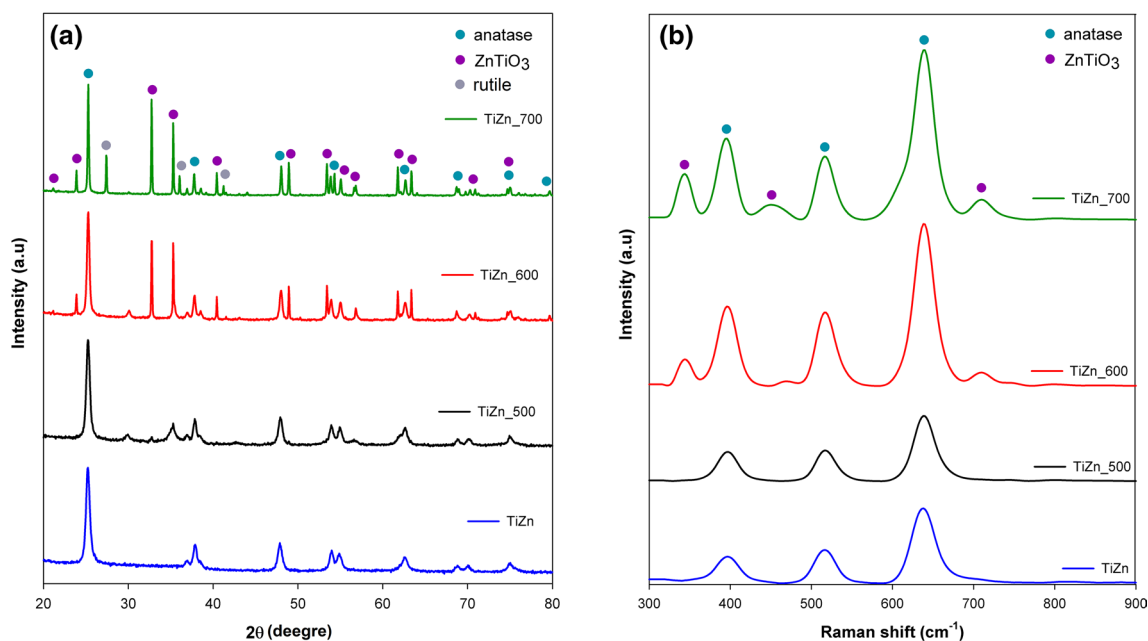
**Fig. 3** XRD patterns (**a**) and Raman spectra (**b**) for $TiO_2$–ZnO system and its thermally treated derivatives

48.9, 52.9, 55.6, 56.71, 61.73, 63.41, 68.73, 70.91 and 74.62. The oxide system calcined at 700 °C has a very similar crystalline structure to the material calcined at 600 °C. The same diffraction reflections from anatase and zinc titanate are observed. In addition, the crystalline structure of rutile (JCPDS No. 21-1279) is observed on the XRD pattern of the TiZn_700 sample. Peaks derived from rutile occur at 2θ values of 27.4, 36.11 and 41.1.

Analysis of the X-ray diffraction results revealed the influence of calcination temperature on the crystalline structure. It was found that the material subjected to hydrothermal treatment contained only an anatase structure, while the binary oxide materials that had undergone calcination exhibited the crystalline structures of anatase, zinc titanate and (in the case of TiZn_700) rutile.

It has been demonstrated in the literature that the addition of ZnO inhibits the formation of the $TiO_2$ crystal structure (Chen et al. 2014; Giannakopoulou et al. 2014); therefore in our study we used a small quantity of ZnO (molar ratio $TiO_2$:ZnO = 8:2). Furthermore, many researchers, such as Cheng et al. (2016) and Xu et al. (2011), who synthesized $TiO_2$–ZnO binary oxide systems using a hydrothermal method, have shown that a small addition of ZnO does not affect the observation of the wurtzite structure on the XRD pattern. However, the additional calcination process influences the formation of the structure of zinc titanate ($ZnTiO_3$) (Tolba et al. 2015). Raveendra et al. (2014) and Chang et al. (2004) also reported that the calcination process influences the formation of the $ZnTiO_3$ structure. However, in the cited works a zinc titanate crystalline structure was obtained only

at 700 °C, while in our study a well-formed crystalline structure was observed at 600 °C. Wang et al. (2011) found that an increase in calcination temperature to 900 °C leads to the formation of other forms of zinc titanate ($Zn_2TiO_4$ and $Zn_2Ti_3O_8$).

To confirm the XRD results concerning the crystalline structure, Raman spectroscopy was carried out. Figure 3b shows the Raman spectra for $TiO_2$–ZnO binary oxide systems subjected to hydrothermal treatment and calcination-assisted processes.

The Raman spectrum for TiZn contains only characteristic bands for anatase, with peaks at wavenumbers 395, 510 and 640 $cm^{-1}$ (Nolan et al. 2011; Sedpho et al. 2008). It was shown that the material calcined at 500 °C (TiZn_500) has a similar crystalline structure to the TiZn sample. For the material subjected to calcination at 600 °C, two additional bands are observed compared with the previously described samples. For TiZn_600, peaks characteristic of anatase were observed at the wavenumbers 395, 510 and 640 $cm^{-1}$, while $ZnTiO_3$ bands are also present at 350 and 710 $cm^{-1}$ (Nolan et al. 2011; Sedpho et al. 2008). An increase in calcination temperature to 700 °C improves the parameters of the crystalline structure; in this case an additional peak at 480 $cm^{-1}$, derived from zinc titanate, was observed.

The influence of calcination temperature on the crystalline structure has therefore been demonstrated. Also, the results from Raman spectroscopy are consistent with those of X-ray diffraction. Similar results to those presented here have been obtained by many researchers. Araújo et al. (2016) synthesized a $TiO_2$–ZnO oxide system via an electrospinning

method. They observed bands characteristic for anatase, wurtzite and zinc titanate. The studies by Ehsan et al. (2015) and Krylova et al. (2010) showed the presence of bands characteristic for $TiO_2$ and $ZnTiO_3$.

The current state of scientific knowledge indicates that oxide materials of the $TiO_2$–ZnO type feature the coexistence of such crystalline structures as rutile and $ZnTiO_3$, as well as anatase, $Zn_2TiO_4$ and $Zn_2Ti_3O_8$ (Konyar et al. 2012; Yamaguchi et al. 1987). The presence of specific crystalline structures is also determined by the starting materials (Liu et al. 2009). Dulin and Rase (1960) indicate that at a specific molar ratio of $TiO_2$:ZnO, a specific crystalline structure is formed. Moreover, with the molar ratio $TiO_2$:ZnO = 8:2 adopted in this work, according to literature data, we should obtain anatase and $Zn_2TiO_4$, which is not observed on the diffraction patterns we obtained. Similar results as described by Dulin and Rase (1960) were obtained by Mehrabi and Javanbakht (2018), who obtained a $TiO_2$–$ZnTiO_3$ material characterized by the crystal structure of rutile and zinc titanate. The synthesis method proposed in this study, which used hydrothermal treatment in the first stage, followed by the calcination process, made it possible to combine the structure of anatase and zinc titanate, which has not been previously described for similar materials.

Figure 4 shows the DR/UV–Vis adsorption spectra of wavelength absorbance for the binary $TiO_2$–ZnO photocatalysts.

The TiZn sample exhibited only UV absorption. For the remaining materials (TiZn_500, TiZn_600 and TiZn_700) two radiation absorption bands were observed, the first in the visible light range (390–600 nm) and the second in the UV range (250–380 nm). In addition, the calcination temperature was found to affect the increase in absorbance in the visible and UV ranges. These results are in agreement
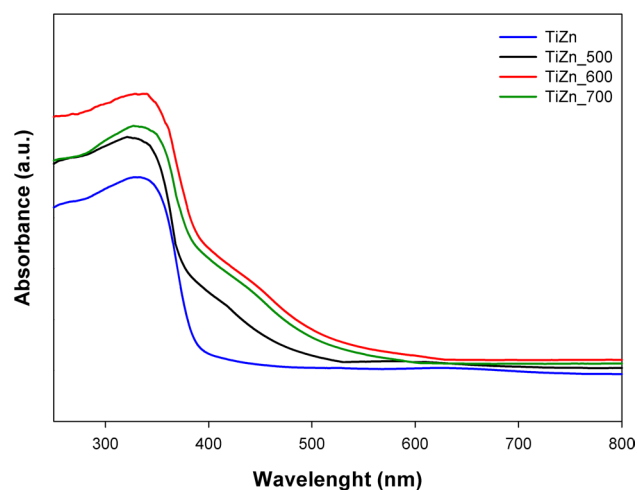
with the XRD results. It is assumed that the presence of the $ZnTiO_3$ crystalline structure influences the increase in absorption in the wavelength range 200–600 nm. Similar effects of the addition of $ZnTiO_3$ have been reported by other researchers (Habibi et al. 2012; Kong et al. 2009; Perween and Ranjan 2017; Yan et al. 2015). Many reports refer to the properties of $ZnTiO_3$ as a visible light active photocatalyst (Anpo and Takeuchi 2003; Reddy et al. 2013; Surendar et al. 2014; Zhang et al. 2012). Based on the DR/UV–Vis analysis and literature knowledge, it is found that the obtained oxide materials have a wide absorption band in the range of 390–600 nm, which enables them to be used in the degradation of organic pollutants in visible light. The energy band gap of the semiconductor samples was calculated by Kubelka–Munk theory. The band gap energies for TiZn, TiZn_500, TiZn_600 and TiZn_700 were found to be 3.2, 3.1, 3.0 and 3.0 eV respectively (Table 2). The value of the band gap for the sample TiZn is similar to the values obtained for $TiO_2$ in other studies (Dette et al. 2014; Kumar and Devi 2011; Kuvarega and Mamba 2017; Pelaez et al. 2012; Zaleska 2008). For the oxide system calcined at 500 °C (TiZn_500), a change in band gap energy was observed. This is related to the formation of the $ZnTiO_3$ structure. Both materials TiZn_600 and TiZn_700 had a band gap equal to 3.0 eV, which is close to values reported for the $ZnTiO_3$ band gap (Lei et al. 2017; Salavati-Niasari et al. 2016; Yan et al. 2015).

To determine the composition of the oxide compounds on the surface of the obtained materials, X-ray fluorescence with energy dispersion (EDXRF) analysis was carried out. Figure 5 shows EDXRF spectra for all of the $TiO_2$–ZnO binary oxide systems.

The EDXRF spectra show that all of the materials (TiZn, TiZn_500, TiZn_600 and TiZn_700) have similar contents of titanium dioxide (84%) and zinc oxide (16%). Furthermore, it was observed that the assumed molar ratio of $TiO_2$:ZnO = 8:2 is close to the experimental value.

Figure 6 shows the results of low-temperature nitrogen sorption. Porous structure parameters—BET surface area, pore volume and pore diameter—of the synthesized materials are presented in Table 3.

The nitrogen adsorption/desorption isotherms correspond to type-IV isotherms (Sing et al. 1985), which indicate the



**Fig. 4** DR-UV/Vis spectra of wavelength absorbance for TiZn, TiZn_500, TiZn_600 and TiZn_700

**Table 2** Energy band gap for obtained binary oxide systems

| Materials | Energy band gap (eV) |
|-----------|---------------------|
| TiZn | 3.2 |
| TiZn_500 | 3.1 |
| TiZn_600 | 3.0 |
| TiZn_700 | 3.0 |
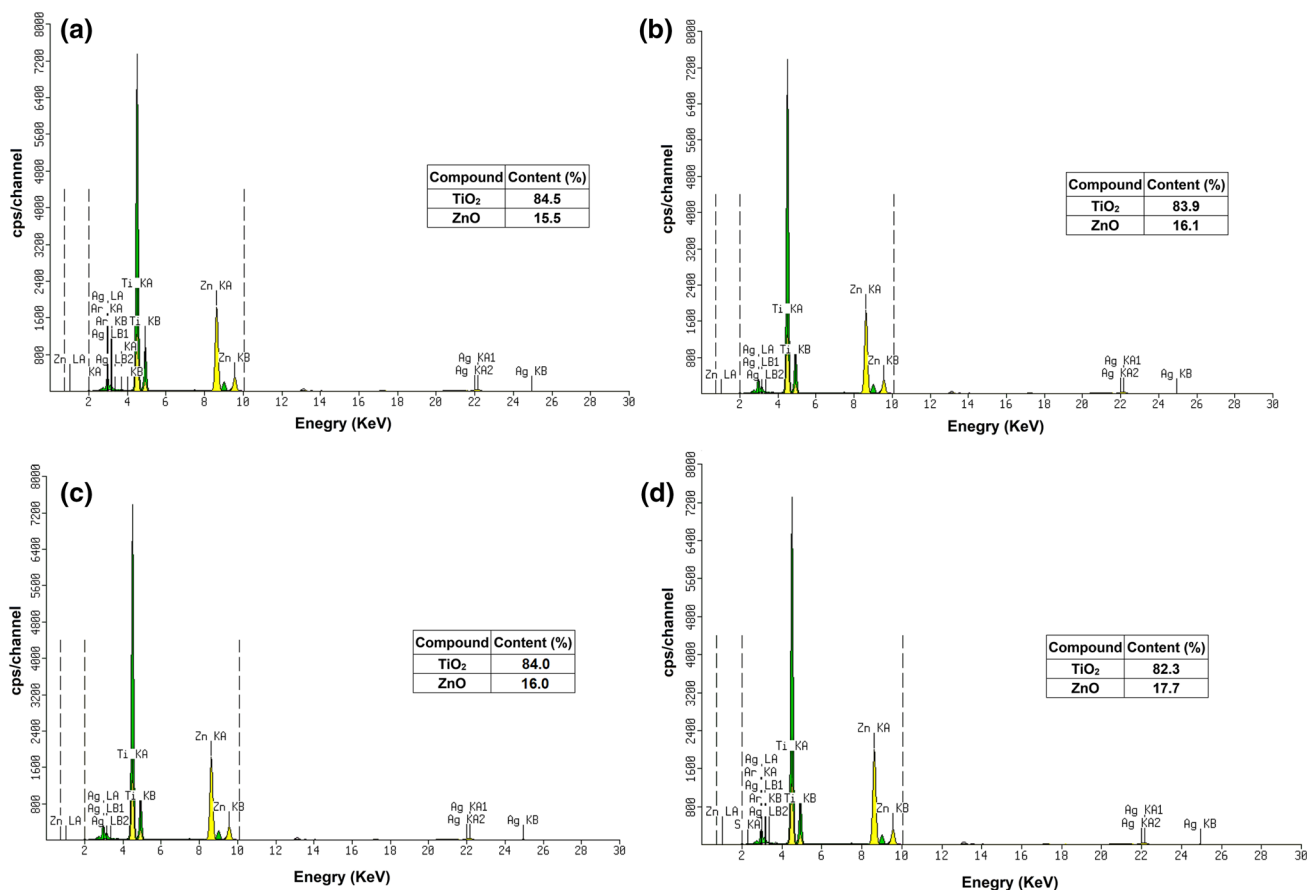
**Fig. 5** EDXRF spectra of **a** TiZn, **b** TiZn_500, **c** TiZn_600 and **d** TiZn_700



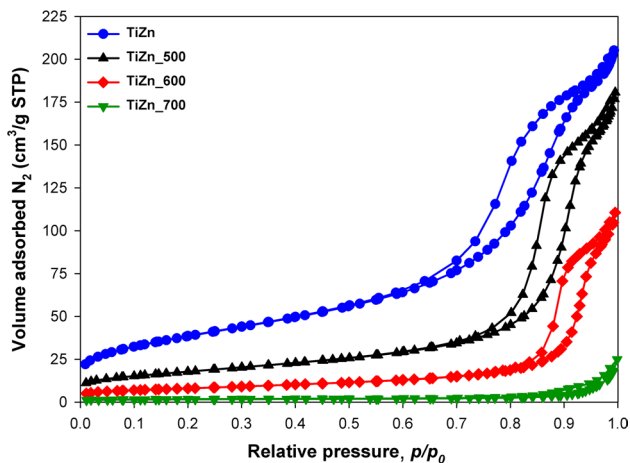**Fig. 6** $N_2$ adsorption/desorption isotherms of the obtained binary oxide systems

mesoporous nature of the $TiO_2$–ZnO binary oxide materials. Desorption hysteresis loops for the synthesized $TiO_2$–ZnO binary oxide systems appear when the relative pressure ($p/p_0$) lies in the range from 0.6 to 0.99 (TiZn), 0.72 to 0.99 (TiZn_500), 0.83 to 0.99 (TiZn_600) or 0.9 to

**Table 3** Parameters of the porous structure of $TiO_2$–ZnO oxide systems

| Sample | $A_{BET}$ ($m^2$/g) | $V_p$ ($cm^3$/g) | $S_p$ (nm) |
|---|---|---|---|
| TiZn | 137.8 | 0.310 | 8.8 |
| TiZn_500 | 63.1 | 0.270 | 15.8 |
| TiZn_600 | 28.1 | 0.170 | 22.9 |
| TiZn_700 | 5.3 | 0.037 | 40.8 |

0.99 (TiZn_700). The hysteresis type of the isotherms can be classified as H1 (Sing et al. 1985), which is related to the capillary condensation associated with the mesoporous channels of $TiO_2$–ZnO oxide systems.

The porous structure analysis showed that the material TiZn (with only hydrothermal treatment at 200 °C) has a relatively high surface area ($A_{BET}$ = 137.8 $m^2$/g). This material also has a pore volume ($V_p$) of 0.310 $cm^3$/g and a pore diameter ($S_p$) of 8.8 nm. Materials subjected to the calcination process have lower BET surface area and pore volume, and higher pore diameter. The $TiO_2$–ZnO oxide system assisted by calcination at 500 °C had a BET surface area of 63.1 $m^2$/g and a pore volume and pore diameter of 0.270 $cm^3$/g and

15.8 nm respectively. Slightly poorer porous structure parameters were observed for sample TiZn_600, which had a BET surface area ($A_{BET}$) of 28.1 m$^2$/g, pore volume 0.170 cm$^3$/g, and pore diameter 22.9 nm. The poorest parameters were those of the material TiZn_700, for which the surface area was 5.3 m$^2$/g, and the pore volume ($V_p$) and pore diameter ($S_p$) were 0.037 cm$^3$/g and 40.8 nm.

These results show that the calcination process causes a significant reduction in the BET surface area. This effect is commonly reported in the literature (Castro and Benthem 2013; Iatsenko et al. 2015), and results from the fact that sintering occurs and causes the closure of pores. Calcination also causes a decrease in pore volume ($V_p$) and an increase in pore diameter ($S_p$). The sintering effect was also observed in the TEM analysis (Fig. 2). Closure of the porous structure was observed, together with an increase in particle size, as the temperature of calcination increased.

Cheng et al. (2016) synthesized TiO$_2$–ZnO oxide systems using a two-stage hydrothermal method. BET analysis of the resulting materials showed them to have a large surface area ($A_{BET}$ = 122–392 m$^2$/g). The material with the largest BET surface area ($A_{BET}$ = 392 m$^2$/g) contained only the crystalline structure of anatase, while the smallest surface area ($A_{BET}$ = 122 m$^2$/g) was observed for a material with the crystalline structure of anatase and wurtzite. It was reported that the improvement of the crystalline structure parameters was related to the decrease in the BET surface area. Another research team (Al-Mayman et al. 2017) studied the use of a TiO$_2$–ZnO oxide system in the photocatalytic production of hydrogen. For the synthesis of the material, they used the sol–gel method and calcination at 500 °C. It was shown that an oxide material similar to that synthesized in the present study had a BET surface area in the range 52.08–36.64 m$^2$/g. The largest surface area was observed for the material with a ZnO content of 1%, and the smallest for the material with the highest ZnO content (30%). With increasing ZnO content, the formation of the anatase crystal structure deteriorated. Wang et al. (2010) obtained a TiO$_2$–ZnO oxide system using the sol–gel method and calcination at different temperatures; the resulting system was found to have a surface area of 76.25 m$^2$/g, a pore volume of 0.012 cm$^3$/g and a pore diameter of 6.6 nm. This material contained the crystalline structures of anatase and wurtzite. Based on these reports (Al-Mayman et al. 2017; Cheng et al. 2016; Wang et al. 2010) it may be concluded that the improvement of the parameters of the crystalline structure is related to the decrease in the BET surface area.

The last stage of the physicochemical analysis was the identification of characteristic functional groups. FT-IR spectra of the TiO$_2$–ZnO binary oxide systems subjected to hydrothermal and calcination treatment are shown in Fig. 7, in a wavenumber range from 4000 to 400 cm$^{-1}$.
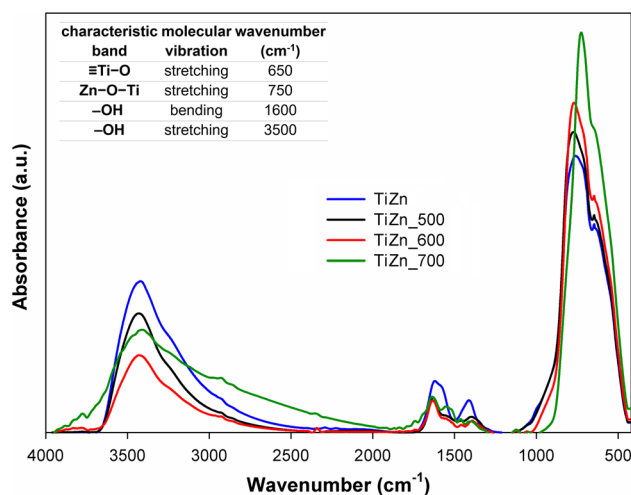


**Fig. 7** FT-IR spectra of TiO$_2$–ZnO binary oxide systems subjected to hydrothermal treatment and calcination

The FT-IR spectra for all of the materials contained four characteristic bands: for stretching vibrations of ≡Ti–O (650 cm$^{-1}$) (Lotus et al. 2011) and Zn–O–Ti (750 cm$^{-1}$) (Moradi et al. 2012), and for hydroxyl group (–OH) bending vibrations (1600 cm$^{-1}$) (Pozan and Kambur 2014) and stretching vibrations (3500 cm$^{-1}$) (Pozan and Kambur 2014). The calcination temperature was found to influence the intensity of the characteristic bands for Ti–O and Zn–O–Ti. The FT-IR analysis proved the effectiveness of the proposed synthesis methodology.

### 3.2 Analysis of photocatalytic activity

Titanium dioxide is widely known for its photocatalytic properties. Due to its band gap of 3.2 eV, it can be used in the UV radiation range. In this study we used zinc oxide to improve the photocatalytic properties of titania and enable photodegradation in visible light. Figure 8 shows the degradation curves of the model organic pollutants—C.I. Basic Blue 3, C.I. Basic Red 1, C.I. Basic Violet 10 and 4-nitrophenol—using the obtained photocatalysts. These impurities were selected for the photodegradation process because they are common organic pollutants found in wastewater (Jin et al. 2007; Kang et al. 2009; Miranda et al. 2013; Peretz and Cinteza 2008).

The first process used to assess the photocatalytic properties of the synthesized materials was the degradation of C.I. Basic Blue 3 (Fig. 8a). For the material TiZn (subjected to hydrothermal treatment only) the degradation yield was approximately 55% after 360 min. The system subjected to calcination at 500 °C (TiZn_500) exhibited improved photocatalytic properties, with a degradation yield of about 97% after 360 min. In the case of the materials subjected to calcination at 600–700 °C a significant increase in degradation
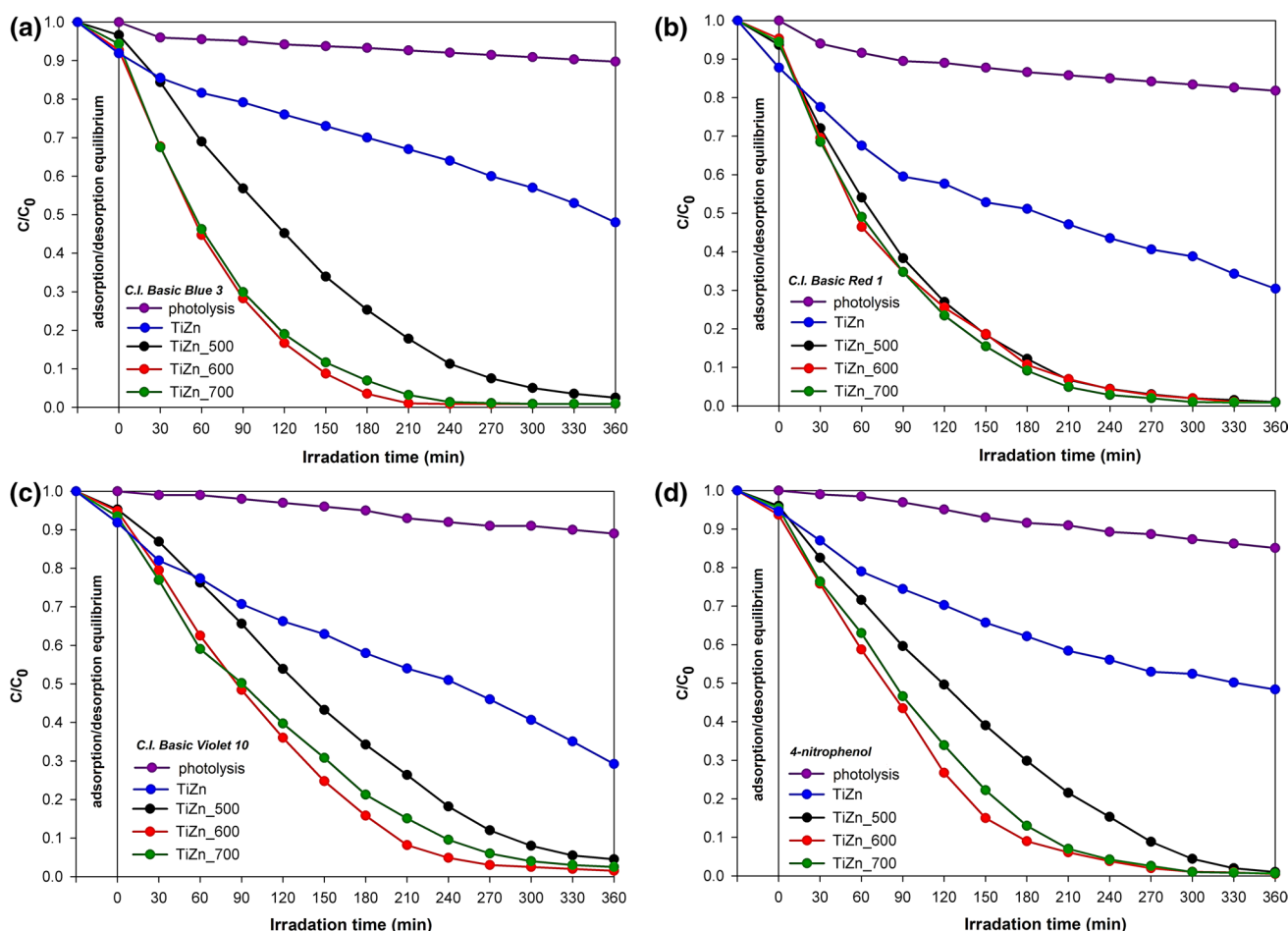
**Fig. 8** Degradation curves of model organic pollutants: **a** C.I. Basic Blue 3, **b** C.I. Basic Red 1, **c** C.I. Basic Violet 10 and **d** 4-nitrophenol

of the organic pollutant was observed: the degradation yield after 180 min was 96% for TiZn_600 and 91% for TiZn_700. During the experiments, photolysis of the degraded dye was observed. It was calculated that the yield of degradation under the influence of light is about 10% after irradiation for 360 min. The observed significant increase in photocatalytic activity may be related to the improved crystalline structure properties of the synthesized materials.

In the second stage of evaluation of the photocatalytic activity of the obtained binary oxide systems, C.I. Basic Red 1 was decolorized (Fig. 8b). The material subjected only to hydrothermal treatment at 200 °C (TiZn) produced a degradation yield of 70% after 360 min. It was found that all materials subjected to calcination, regardless of temperature, gave a degradation yield of about 90% after 180 min. In contrast to the case of C.I. Basic Blue 3, no effect of calcination temperature on photodegradation performance was observed. The yield of C.I. Basic Red 1 photolysis was demonstrated to be 14.3% after 360 min.

Next, C.I. Basic Violet 10 degradation was investigated (Fig. 8c). Substances in this group are common

organic pollutants, being used as fluorescent dyes (Carneiro et al. 2016; Pei and Leung 2013). The yield of C.I. Basic Violet 10 decomposition obtained with TiZn was 70% after 360 min. However, a significant improvement in photocatalytic activity was demonstrated for the calcined materials. The decoloration yield after 210 min was 73.5%, 91.8% and 84.5% for TiZn_500, TiZn_600 and TiZn_700 respectively. The yield of degradation of the pollutant under visible light was measured at 11.2% after 360 min.

The final stage of the broad-ranging analysis of photocatalytic activity involved the degradation of 4-nitrophenol (Fig. 8d). For the reference material (TiZn), the degradation yield was 51.6% after 360 min. With the material subjected to calcination at 500 °C (TiZn_500) the yield was 99% after 360 min. In the presence of TiZn_600 the yield of degradation of 4-nitrophenol was 91% after 180 min, and with the last synthesized material (TiZn_700) the yield was 87% after 180 min. The yield of photolysis was found to be 14.9% after 360 min.

The tests of photocatalytic activity show that all of the synthesized TiO$_2$–ZnO binary oxide systems demonstrate

a high efficiency of photodegradation of organic impurities. It was found that the calcination-assisted materials have higher photocatalytic efficiency than the material subjected to hydrothermal treatment only. This is probably due to the improvement of the crystalline structure parameters. An increase in the calcination temperature to 600 °C causes the formation of the crystalline structure of zinc titanate ($ZnTiO_3$), which is linked to an improvement in photocatalytic activity. Many researchers have described the very good photocatalytic properties of $ZnTiO_3$ in visible light (Perween and Ranjan 2017; Regupathi et al. 2016; Yan et al. 2015). The material calcined at 700 °C (TiZn_700) has slightly poorer photooxidation properties for the photodegradation of organic pollutants, because the XRD pattern reveals diffraction peaks from the rutile crystalline structure, which is considered to reduce the efficiency of photodegradation. The results show that the synthesized $TiO_2$–ZnO binary oxide systems may be promising materials for the degradation of organic pollutants in visible light. Furthermore, a relationship between photocatalytic activity and morphology and BET surface area was demonstrated. It was observed that the increase in photodegradation efficiency is associated with a decrease in the BET surface area, which in turn is associated with the closure of the porous surface and an increase in particle size caused by the sintering effect.

Khataee et al. (2011) also investigated the degradation of C.I. Basic Blue 3 using $TiO_2$ and UV light for the decomposition process. The photocatalysis process was carried out for 480 min, but even after 120 min a high photodegradation yield (90%) was observed. Buyukada (2016) used titanium dioxide for the photodegradation of C.I. Basic Blue 3. The degradation yield (determined by chemical oxygen demand) was shown to be 88%.

Ghorai and Biswas (2013) used a $TiO_2$–$SrCrO_4$ oxide system to decolor C.I. Basic Red 1 (concentration $10^{-3}$ M) under UV light. The high photocatalytic activity of the system was demonstrated: the degradation yield reached 100% after 5 h. Chong et al. (2015) studied the degradation of C.I. Basic Red 1 (concentration $10^{-5}$ M) in UV light using Ag-modified $TiO_2$, and observed total decomposition of the solution after 120 min.

Literature reports show that C.I. Basic Violet 10 is a common organic pollutant used to assess photocatalytic activity (Du et al. 2013; Natarajan et al. 2011; Pei and Leung 2013; Siwińska-Stefańska et al. 2018; Zhang et al. 2011). Titanium dioxide and $TiO_2$–ZnO oxide systems are commonly used for the degradation of compounds of this type in both UV and visible light. Carneiro et al. (2016) showed the good photocatalytic activity of functionalized $TiO_2$ in the decomposition of C.I. Basic Violet 10 solution (4 mg/dm$^3$), obtaining a degradation yield of almost 100% after approximately 300 min. Pei and Leung (2013) used a $TiO_2$–ZnO oxide system in the
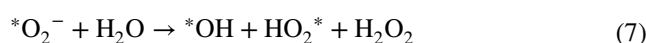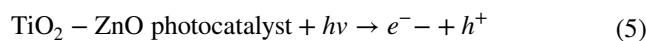
photodegradation of C.I. Basic Violet 10. They showed the high photoactivity of that material in visible light, with a 100% degradation yield in a time of 100 min.

Many studies have demonstrated the good properties of modified $TiO_2$ in the photodegradation of 4-nitrophenol solution. Gaffour and Mokhtari (2016) described the degradation of 4-nitrophenol (20 mg/dm$^3$) using $TiO_2$–$Fe_2O_3$ as a photocatalyst. A high photodegradation yield (98%) was obtained after 180 min. Yang et al. (2010) carried out degradation using $TiO_2$–$Cu_2O$ in visible light, and observed complete photodegradation of 4-nitrophenol after 210 min.

A review of the literature shows that our work on the photodegradation of model organic pollutants has produced higher photocatalytic efficiency than previous studies. The use of zinc citrate as a ZnO precursor made it possible to obtain materials with a mixed anatase-$ZnTiO_3$ crystalline structure, which directly affected the results of photodegradation.

The mechanism of degradation of pollutants such as dyes or phenol derivativesis widely known in the scientific literature. Many scientists (Gayathri et al. 2015; Perween and Ranjan 2017; Sirajudheen et al. 2016; Surendar et al. 2014; Yan et al. 2015) describe the mechanism of degradation using $ZnTiO_3$ and $TiO_2$ as photocatalysts. On this basis we propose a possible mechanism and reactions for the photodegradation of organic pollutants in the presence of the synthesized materials.

The zinc titanate irradiated under visible light causes electron transport from the valence band (VB) to the conduction band (CB), leaving an equal number of vacant sites (holes). The influence of $Zn^{2+}$ ions is described as that of electron traps retarding electron–hole recombination, which affects improve the hole transfer required to degrade the organic impurities adsorbed on the surface of the photocatalyst particles. Moreover, electrons may be transferred from the conduction band to the dissolved oxygen, leading to superoxide anion radicals ($^*O_2^-$) which in the next step could be transformed to active oxygen species, such as $HO_2^*$, $^*OH$ and $H_2O_2$. Next, the holes at the valence band of the photocatalyst react with adsorbed water or surface hydroxyl groups ($-OH^-$) to produce $^*OH$ radicals. These $^*OH$ radicals and the holes are considered to be the main elements causing photodegradation of organic pollutants (Bhatkhande et al. 2002; Liu et al. 2013; Tang et al. 2013). The major steps in the mechanism of photocatalytic decomposition are shown in the equations below:

$$TiO_2 - ZnO \ photocatalyst + hv \rightarrow e^- - + h^+ \tag{5}$$

$$e^- + O_2 \rightarrow {}^*O_2^- \tag{6}$$

$$^*O_2^- + H_2O \rightarrow {}^*OH + HO_2{}^* + H_2O_2 \tag{7}$$

$$h^+ + H_2O/OH^- \rightarrow H^+ + OH^* \tag{8}$$

$^{*}$OH or $h^{+}$ + organic pollutant → degradation products

$$(9)$$

Figure 9 gives a graphical representation of the mechanism of photodegradation of the organic pollutants.

Results of the kinetic study of the photocatalysis process in the presence of selected catalysts are presented in Table 4.

Analysis of the kinetics of photooxidation of C.I. Basic Blue 3 shows that the constant rate of degradation was higher in the presence of TiZn_600 (0.0132 1/min) and TiZn_700 (0.0131 1/min) compared with the other analyzed photocatalysts. Moreover, decomposition of this impurity was characterized by the shortest half-life (52 min) when the aforementioned samples were applied as photocatalysts. Heterogeneous photodegradation of C.I. Basic Blue 3 in the presence of samples TiZn_500 and TiZn had a lower constant rate of reaction (0.0102 and 0.002 1/min respectively) and a longer half-life (67 and 319 min).

Analogous patterns were observed in the decomposition of the other three organic pollutants in the presence of TiO$_2$–ZnO oxide materials. Decomposition of C.I. Basic Red 1 in the presence of the synthesized photocatalysts produced similar values of constant rate and half-life in comparison with the photooxidation of C.I. Basic Blue 3. The constant rate of degradation of C.I. Basic Red 1 in the presence of TiZn_600 and TiZn_700 was 0.0131 1/min, and the half-life was 53 min. A slightly lower constant rate of degradation was recorded when the photooxidation process was carried out in the presence of TiZn_500 photocatalyst (0.0128 1/min).
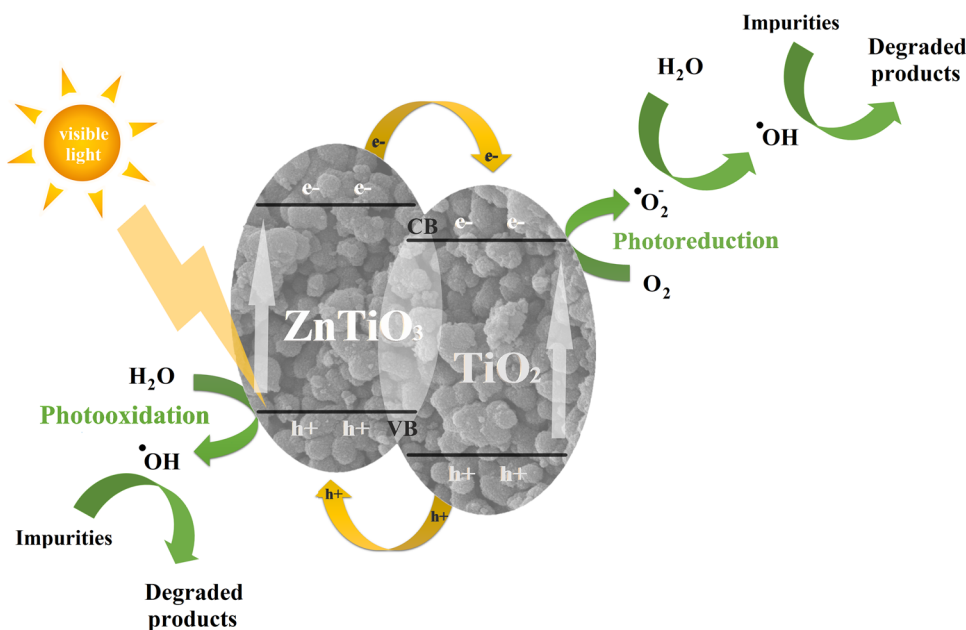
The lowest values of the constant rate of reaction were recorded when the synthesized materials were applied in

**Table 4** The reaction rate constant ($k$), correlation coefficient ($R^2$) and half-life time ($t_{1/2}$) of selected organic-based impurities during photocatalytic process

| Sample | $k$ (1/min) | $R^2$ | $t_{1/2}$ (min) |
|---|---|---|---|
| C.I. Basic Blue 3 | | | |
| TiZn | 0.0022 | 0.8903 | 319.73 |
| TiZn_500 | 0.0102 | 0.9562 | 67.64 |
| TiZn_600 | 0.0132 | 0.9533 | 52.48 |
| TiZn_700 | 0.0131 | 0.9817 | 52.98 |
| C.I. Basic Red 1 | | | |
| TiZn | 0.0033 | 0.8161 | 209.63 |
| TiZn_500 | 0.0128 | 0.9887 | 54.18 |
| TiZn_600 | 0.0131 | 0.9929 | 52.96 |
| TiZn_700 | 0.0131 | 0.9840 | 52.96 |
| C.I. Basic Violet 10 | | | |
| TiZn | 0.0034 | 0.9210 | 202.79 |
| TiZn_500 | 0.0086 | 0.9357 | 80.48 |
| TiZn_600 | 0.0117 | 0.9295 | 59.41 |
| TiZn_700 | 0.0117 | 0.9627 | 59.07 |
| 4-Nitrophenol | | | |
| TiZn | 0.0020 | 0.8985 | 341.95 |
| TiZn_500 | 0.0134 | 0.9146 | 51.62 |
| TiZn_600 | 0.0149 | 0.9783 | 46.63 |
| TiZn_700 | 0.0153 | 0.9321 | 45.44 |

photooxidation of C.I. Basic Violet 10. The constant rates of degradation were 0.0034 1/min (TiZn), 0.0086 1/min (TiZn_500) and 0.0117 1/min (TiZn_600 and TiZn_700). The values of the half-life of decomposition of C.I. Basic Violet 10 were in the range 59–203 min.

**Fig. 9** Mechanism of photocatalytic degradation of organic impurities

The highest values of the constant rate of decomposition were observed in the degradation process of 4-nitrophenol performed in the presence of the synthesized materials. The values were as follows: 0.0020 1/min (TiZn), 0.0134 1/min (TiZn_500), 0.0149 1/min (TiZn_600) and 0.0153 1/min (TiZn_700). In this case the half-life values lay in the range 45–341 min.

The results show clearly that higher values of the constant rate of reaction and shorter half-lives were recorded when the materials TiZn_600 and TiZn_700 were used in the decomposition of the selected organic pollutants. It would appear that the higher photoactivity of materials calcined at higher temperatures (600 and 700 °C) is related to the presence of the ZnTiO₃ phase in their structure, which may significantly affect their photocatalytic behaviour.

## 4 Conclusions

The main objective of this work was the synthesis of a TiO$_2$–ZnO oxide system using a ZnO precursor that had not previously been described: zinc citrate. The use of a new type of ZnO precursor made it possible to obtain the crystalline structure of anatase and ZnTiO$_3$. During the study, the influence of the calcination temperature on the physicochemical and structural properties of the obtained materials was determined. All of the synthesized photocatalysts were characterized by a spherical particle shape with agglomeration. For the calcined products, closure of the porous structure and an increase in particle size were observed, this being associated with sintering. An increase in the temperature of calcination influenced the crystalline structure of zinc titanate (ZnTiO$_3$) and caused a decrease in the BET surface area. The obtained FT-IR spectra contained bands characteristic for Zn–O–Ti, ≡Ti–O and –OH groups.

The key element of the research was the evaluation of the efficiency of photodegradation of the model organic pollutants C.I. Basic Blue 3, C.I. Basic Red 1, C.I. Basic Violet 10 and 4-nitrophenol. The materials subjected to calcination exhibited high photocatalytic activity in visible light. All of the analyzed organic pollutants were significantly degraded (by approximately 90%) after 180 min. The improvement in photocatalytic activity may be caused by the presence of the crystalline structure of zinc titanate, because ZnTiO$_3$ is widely known for its photocatalytic properties. The results show the synthesized oxide materials to be promising photocatalysts for the degradation of organic pollutants in visible light.

## References

Al-Mayman, S.I., Al-Johani, M.S., Mohamed, M.M., Al-Zeghayer, Y.S., Ramay, S.M., Al-Awadi, A.S., Soliman, M.A.: TiO₂-ZnO photocatalysts synthesized by sol–gel auto-ignition technique for hydrogen production. Int. J. Hydrogen Energy **42**, 5016–5025 (2017)

Anpo, M., Takeuchi, M.: The design and development of highly reactive titanium oxide photocatalysts operating under visible light irradiation. J. Catal. **216**, 505–516 (2003)

Antecka, K., Zdarta, J., Siwińska-Stefańska, K., Sztuk, G., Jankowska, E., Oleskowicz-Popiel, P., Jesionowski, T.: Synergistic degradation of dye wastewaters using binary or ternary oxide systems with immobilized laccase. Catalysts **8**, 402 (2018)

Araújo, E.S., da Costa, B.P., Oliveira, R.A.P., Libardi, J., Faia, P.M., De Oliveira, H.P.: TiO₂/ZnO hierarchical heteronanostructures: synthesis, characterization and applicationas photocatalysts. J. Environ. Chem. Eng. **4**, 2820–2829 (2016)

Bartczak, P., Norman, M., Klapiszewski, Ł, Karwańska, N., Kawalec, M., Baczyńska, M., Wysokowski, M., Zdarta, J., Ciesielczyk, F., Jesionowski, T.: Removal of nickel(II) and lead(II) ions from aqueous solution using peat as a low-cost adsorbent: a kinetic and equilibrium study, Arab. J. Chem. 1209–1222 (2015)

Bhatkhande, D.S., Pangarkar, V.G., Beenackers, A.A.C.M.: Photocatalytic degradation for environmental applications—a review. J. Chem. Technol. Biotechnol. **77**, 102–116 (2002)

Buyukada, M.: Prediction of photocatalytic degradation and mineralization efficiencies of Basic Blue 3 using TiO₂ by nonlinear modeling based on box–behnken design. Arab. J. Sci. Eng. **41**, 2631–2646 (2016)

Carneiro, J.O., Samantilleke, A.P., Parpot, P., Fernandes, F., Pastor, M., Correia, A., Luís, E.A., Barros, A.A.C., Teixeira, V.: Visible light induced enhanced photocatalytic degradation of industrial effluents (Rhodamine B) in aqueous media using TiO₂ nanoparticles, J. Nanomater. **2016**, 4396175 (2016)

Castro, R.H.R., van Benthem, K.: Sintering, mechanisms of convention nanodensification and field assisted processes. Eng. Mater. (2013). https://doi.org/10.1007/978-3-642-31009-6

Chang, Y.S., Chang, Y.H., Chen, I.G., Chen, G.J., Chai, Y.L., Fang, T.H., Wu, S.: Synthesis, formation and characterization of ZnTiO₃ ceramics. Ceram. Int. **30**, 2183–2189 (2004)

Chen, X., Burda, C.: The electronic origin of the visible light absorption properties of C-, N- and S-doped TiO₂ nanomaterials. J. Am. Chem. Soc. **130**, 5018–5019 (2008)

Chen, D., Ray, A.K.: Photodegradation kinetics of 4-nitrophenol in TiO₂ suspension. Water Res. **32**, 3223–3234 (1998)

Chen, Y., Zhang, C., Huang, W., Yang, C., Huang, T., Situ, Y., Huang, H.: Synthesisof porous ZnO/TiO₂ thin films with superhydrophilicity and photocatalytic activity via a template-free sol-gel method. Surf. Coat. Technol. **258**, 531–538 (2014)

Chen, Y.C., You, H.M., Chang, K.C.: Influence of Li₂WO₄ aid and sintering temperature on microstructures and microwave dielectric properties of Zn₂SnO₄ ceramics. Ceram. Int. **41**, 5257–5262 (2015)

Cheng, P., Wang, Y., Xu, L., Sun, P., Su, Z., Jin, F., Liu, F., Sun, Y., Lu, G.: 3D TiO₂/ZnO composite nanospheres as an excellent electron transport anode for efficient dye-sensitized solar cells. RSC Adv. **6**, 51320–51326 (2016)

Chong, X., Zhao, B., Li, R., Ruan, W., Yang, X.: Photocatalytic degradation of rhodamine 6G on Ag modified TiO₂ nanotubes:

surface-enhanced Raman scattering study on catalytic kinetics and substrate recyclability. Colloids Surf. A **481**, 7–12 (2015)

Cong, Y., Zhang, J., Chen, F., Anpo, M.: Synthesis and characterization of nitrogen-doped $TiO_2$ nanophotocatalyst with high visible light activity. J. Phys. Chem. C **111**, 6976–6982 (2007)

Delsouz Khaki, M.R., Shafeeyan, M.S., Raman, A.A.A., Daud, W.M.A.W.: Evaluating the efficiency of nano-sized Cu doped $TiO_2$/ZnO photocatalyst under visible light irradiation. J. Mol. Liq. **258**, 354–365 (2018a)

Delsouz Khaki, M.R., Shafeeyan, M.S., Raman, A.A.A., Daud, W.M.A.W.: Enhanced UV–Visible photocatalytic activity of Cu-doped ZnO/$TiO_2$ nanoparticles. J. Mater. Sci. Mater. Electron. **29**, 5480–5495 (2018b)

Dette, C., Pérez-Osorio, M.A., Kley, C.S., Punke, P., Patrick, C.E., Jacobson, P., Giustino, F., Jung, S.J., Kern, K.: $TiO_2$ anatase with a bandgap in the visible region. Nano Lett. **14**, 6533–6538 (2014)

Du, P., Song, L., Xiong, J., Cao, H.: Photocatalytic degradation of Rhodamine B using electrospun $TiO_2$ and ZnO nanofibers: a comparative study. J. Mater. Sci. **48**, 8386–8392 (2013)

Dulin, F.H., Rase, D.E.: Phase equilibria in the system ZnO-$TiO_2$. J. Am. Ceram. Soc. **43**, 125–131 (1960)

Ehsan, M.A., Khaledi, H., Pandikumar, A., Rameshkumar, P., Huang, N.M., Arifin, Z., Mazhar, M.: Nitrite ion sensing properties of $ZnTiO_3$ –$TiO_2$ composite thin films deposited from a zinc–titanium molecular complex. New J. Chem. **39**, 7442–7452 (2015)

Esparza, A.M., Gowda, P.H., Baumhardt, R.L., Marek, T.H., Howell, T.A.: Heat unit availability for cotton productions in the Ogallala Aquifer Region of the United States. J. Cotton Sci. **11**, 110–117 (2007)

Fatimah, I., Novitasari: Preparation of $TiO_2$-ZnO and its activity testin sonophotocatalytic degradation of phenol, IOP Conf. Ser. Mater. Sci. Eng. (2016). https://doi.org/10.1088/1757-899X/107/1/012003

Gaffour, H., Mokhtari, M.: Photocatalytic degradation of 4-nitrophenol using $TiO_2$ + $Fe_2O_3$ and $TiO_2$/$Fe_2O_3$-supported bentonite as heterogeneous catalysts. Res. Chem. Intermed. **42**, 6025–6038 (2016)

Galindo, C., Jacques, P., Kalt, A.: Photooxidation of the phenylazonaphthol AO20 on $TiO_2$: kinetic and mechanistic investigations. Chemosphere **45**, 997–1005 (2001)

Gandhi, V.G., Mishra, M.K., Joshi, P.A.: A study on deactivation and regeneration of titanium dioxide during photocatalytic degradation of phthalic acid. J. Ind. Eng. Chem **18**, 1902–1907 (2012)

Gayathri, S., Jayabal, P., Kottaisamy, M., Ramakrishnan, V.: Synthesis of the graphene-$ZnTiO_3$ nanocomposite for solar light assisted photodegradation of methylene blue. J. Phys. D **48**, 415305 (2015)

Ghorai, T.K., Biswas, N.: Photodegradation of rhodamine 6G in aqueous solution via $SrCrO_4$ and $TiO_2$ nano-sphere mixed oxides. J. Mater. Res. Technol. **2**, 10–17 (2013)

Giannakopoulou, T., Todorova, N., Giannouri, M., Yu, J., Trapalis, C.: Optical and photocatalytic properties of composite $TiO_2$/ZnO thin films. Catal. Today **230**, 174–180 (2014)

Habibi, M.H., Mikhak, M., Zendehdel, M., Habibi, M.: Influence of nanostructured zinc titanate, zinc oxide or titanium dioxide thin film coated on fluorine doped tin oxide as working electrodes for dye-sensitized solar cell. Int. J. Electrochem. Sci. **7**, 6787–6798 (2012)

Henderson, M.A.: A surface science perspective on $TiO_2$ photocatalysis. Surf. Sci. Rep. **66**, 185–297 (2011)

Iatsenko, A., Sych, O., Tomila, T.: Effect of sintering temperature on structure and properties of highly porous glass-ceramics. Process. Appl. Ceram. **2**, 99–105 (2015)

Jin, X.C., Liu, G.Q., Xu, Z.H., Tao, W.Y.: Decolorization of a dye industry effluent by *Aspergillus fumigatus XC6*. Appl. Microbiol. Biotechnol. **74**, 239–243 (2007)

Kang, S.Z., Yang, Y.K., Bu, W., Mu, J.: $TiO_2$ nanoparticles incorporated with $CuInS_2$ clusters: preparation and photocatalytic activity for degradation of 4-nitrophenol. J. Solid State Chem. **182**, 2972–2976 (2009)

Khaki, M.R.D., Shafeeyan, M.S., Raman, A.A.A., Daud, W.M.A.W.: Application of doped photocatalysts for organic pollutant degradation—a review. J. Environ. Manag. **198**, 78–94 (2017). https://doi.org/10.1016/j.jenvman.2017.04.099

Khataee, A.R., Fathinia, M., Aber, S.: Kinetic study of photocatalytic decolorization of C.I. Basic Blue 3 solution on immobilized titanium dioxide nanoparticles. Chem. Eng. Res. Des. **89**, 2110–2116 (2011)

Kolodziejczak-Radzimska, A., Jesionowski, T.: Zinc oxide—from synthesis to application: a review. Materials **7**, 2833–2881 (2014)

Kong, J.Z., Li, A.D., Zhai, H.F., Li, H., Yan, Q.Y., Ma, J., Wu, D.: Preparation, characterization and photocatalytic properties of $ZnTiO_3$ powders. J. Hazard. Mater. **171**, 918–923 (2009)

Konstantinou, I.K., Albanis, T.A.: $TiO_2$-assisted photocatalytic degradation of azo dyes in aqueous solution: kinetic and mechanistic investigations: a review. Appl. Catal. B **49**, 1–14 (2004)

Konyar, M., Yatmaz, H.C., Öztürk, K.: Sintering temperature effect on photocatalytic efficiencies of ZnO/$TiO_2$ composite plates. Appl. Surf. Sci. **258**, 7440–7447 (2012)

Krylova, G., Brioude, A., Ababou-Girard, S., Mrazek, J., Spanhel, L.: Natural superhydrophilicity and photocatalytic properties of sol-gel derived $ZnTiO_3$-ilmenite/r-$TiO_2$ films. Phys. Chem. Chem. Phys. **12**, 15101–15110 (2010)

Kubiak, A., Siwińska-Ciesielczyk, K., Jesionowski, T.: Titania-based hybrid materials with ZnO, $ZrO_2$ and $MoS_2$: a review. Materials **11**, 2295 (2018)

Kumar, S.G., Devi, L.G.: Review on modified $TiO_2$ photocatalysis under UV/visible light: Selected results and related mechanisms on interfacial charge carrier transfer dynamics. J. Phys. Chem. A **115**, 13211–13241 (2011)

Kuvarega, A.T., Mamba, B.B.: $TiO_2$-based photocatalysis: toward visible light-responsive photocatalysts through doping and fabrication of carbon-based nanocomposites. Crit. Rev. Solid State Mater. Sci. **42**, 295–346 (2017)

Lei, S., Fan, H., Ren, X., Fang, J., Ma, L., Liu, Z.: Novel sintering and band gap engineering of $ZnTiO_3$ ceramics with excellent microwave dielectric properties. J. Mater. Chem. C **5**, 4040–4047 (2017)

Li, H., Zhang, W., Guan, L.X., Li, F., Yao, M.M.: Visible light active $TiO_2$-ZnO composite films by cerium and fluorine codoping for photocatalytic decontamination. Mater. Sci. Semicond. Process. **40**, 310–318 (2015)

Liu, Z., Zhou, D., Gong, S., Li, H.: Studies on a basic question of zinc titanates. J. Alloys Compd. **475**, 840–845 (2009)

Liu, X., Tang, Y., Luo, S., Wang, Y., Zhang, X., Chen, Y., Liu, C.: Reduced graphene oxide and $CuInS_2$ co-decorated $TiO_2$ nanotube arrays for efficient removal of herbicide 2,4-dichlorophenoxy-acetic acid from water. J. Photochem. Photobiol. A **262**, 22–27 (2013)

Lotus, A.F., Tacastacas, S.N., Pinti, M.J., Britton, L.A., Stojilovic, N., Ramsier, R.D., Chase, G.G.: Fabrication and characterization of $TiO_2$-ZnO composite nanofibers. Physica E **43**, 857–861 (2011)

Luo, J., Zhang, Y.: Promoting the flash sintering of ZnO in reduced atmospheresto achieve nearly full densities at furnace temperatures of < 120 °C. Scr. Mater. **106**, 26–29 (2015)

Mehrabi, M., Javanbakht, V.: Photocatalytic degradation of cationic and anionic dyes by a novel nanophotocatalyst of $TiO_2$/$ZnTiO_3$/

αFe$_2$O$_3$ by ultraviolet light irradiation. J. Mater. Sci. Mater. Electron. **29**, 9908–9919 (2018)

Miranda, R.C.M., Gomes, E.B., Pereira, N., Marin-Morales, M.A., Machado, K.M.G., Gusmão, N.B.: Biotreatment of textile effluent in static bioreactor by *Curvularia lunata* URM 6179 and *Phanerochaete chrysosporium* URM 6181. Bioresour. Technol. **142**, 361–367 (2013)

Mishra, K.P., Gogate, P.R.: Intensification of sonophotocatalytic degradation ofp-nitrophenol at pilot scale capacity. Ultrason. Sonochem. **18**, 739–744 (2011)

Moradi, S., Aberoomand Azar, P., Raeis Farshid, S., Abedini Khorrami, S., Givianrad, M.H.: Effect of additives on characterization and photocatalytic activity of TiO$_2$/ZnO nanocomposite prepared via sol-gel process, Int. J. Chem. Eng. 2012, 215373 (2012)

Nakata, K., Fujishima, A.: TiO$_2$ photocatalysis: design and applications,J. Photoch. Photobiol. C **13**, 169–189 (2012)

Natarajan, T.S., Thomas, M., Natarajan, K., Bajaj, H.C., Tayade, R.J.: Study on UV-LED/TiO$_2$ process for degradation of Rhodamine B dye. Chem. Eng. J. **169**, 126–134 (2011)

Nie, Z., Lin, Y., Wang, F.: Low-temperature sintering of ZnO–TiO$_2$ ceramics. J. Eng. Mater. Technol. **137**, 31010 (2015)

Nolan, N.T., Seery, M.K., Pillai, S.C.: Crystallization and phase-transition characteristics of sol-gel synthesized zinc titanates. Chem. Mater. **6**, 1496–1504 (2011)

Oghbaei, M., Mirzaee, O.: Microwave versus conventional sintering: A review of fundamentals, advantages and applications. J. Alloys Compd. **494**, 175–189 (2010)

Pandurangan, A., Kamala, P., Uma, S., Palanichamy, M., Murugesan, V.: Degradation of basic yellow auramine O-A textile dye by semiconductor photocatalysis. Indian J. Chem. Technol. **8**, 496–499 (2001)

Pant, H.R., Pant, B., Sharma, R.K., Amarjargal, A., Kim, H.J., Park, C.H., Tijing, L.D., Kim, C.S.: Antibacterial and photocatalytic properties of Ag/TiO$_2$/ZnO nano-flowers prepared by facile one-pot hydrothermal process. Ceram. Int. **39**, 1503–1510 (2013)

Parida, K., Das, D.P.: Photo-oxidation of 4-nitrophenol in aqueous suspensions, catalysed by titania intercalated zirconium phosphate (ZrP) and titanium phosphate (TiP). J. Photoch. Photobio. A **163**, 561–567 (2004)

Pei, C.C., Leung, W.W.F.: Photocatalytic degradation of Rhodamine B by TiO$_2$/ZnO nanofibers under visible-light irradiation. Sep. Purif. Technol. **114**, 108–116 (2013)

Pelaez, M., Nolan, N.T., Pillai, S.C., Seery, M.K., Falaras, P., Kontos, A.G., Dunlop, P.S.M., Hamilton, J.W.J., Byrne, J.A., Shea, K.O., Entezari, M.H., Dionysiou, D.D.: A review on the visible light active titanium dioxide photocatalysts for environmental applications. Appl. Catal. B **125**, 331–349 (2012)

Peretz, S., Cinteza, O.: Removal of some nitrophenol contaminants using alginate gel beads. Colloids Surf. A **319**, 165–172 (2008)

Pérez-González, M., Tomás, S.A., Santoyo-Salazar, J., Morales-Luna, M.: Enhanced photocatalytic activity of TiO$_2$-ZnO thin films deposited by dc reactive magnetron sputtering. Ceram. Int. **43**, 8831–8838 (2017)

Perween, S., Ranjan, A.: Improved visible-light photocatalytic activity in ZnTiO$_3$ nanopowder prepared by sol-electrospinning. Sol. Energy Mater. Sol. Cells **163**, 148–156 (2017)

Pozan, G.S., Kambur, A.: Significant enhancement of photocatalytic activity over bifunctional ZnO-TiO$_2$ catalysts for 4-chlorophenol degradation. Chemosphere **105**, 152–159 (2014)

Rahim Pouran, S., Aziz, A.A., Daud, W.M.A.W., Shafeeyan, M.S.: Effects of niobium and molybdenum impregnation on adsorption capacity and Fenton catalytic activity of magnetite. RSC Adv. **5**, 87535–87549 (2015)

Rahim Pouran, S., Bayrami, A., Aziz, A.A., Daud, W.M.A.W., Shafeeyan, M.S.: Ultrasound and UV assisted Fenton treatment of recalcitrant wastewaters using transition metal-substituted-magnetite nanoparticles. J. Mol. Liq. **222**, 1076–1084 (2016)

Rahim Pouran, S., Bayrami, A., Abdul Raman, A.A., Wan Daud, W.M.A., Shafeeyan, M.S., Khataee, A.: Comprehensive study on the influence of molybdenum substitution on characteristics and catalytic performance of magnetite nanoparticles. Res. Chem. Intermed. **44**, 883–900 (2018a)

Rahim Pouran, S., Bayrami, A., Shafeeyan, M.S., Raman, A.A.A., Daud, W.M.A.: A comparative study on a cationic dye removal through homogeneous and heterogeneous fenton oxidation systems. Acta Chim. Slov. **65**, 166–171 (2018b)

Raveendra, R.S., Prashanth, P.A., Hari Krishna, R., Bhagya, N.P., Nagabhushana, B.M., Raja Naika, H., Lingaraju, K., Nagabhushana, H., Prasad, H., Daruka, B.: Synthesis, structural characterization of nano ZnTiO$_3$ ceramic: an effective azo dye adsorbent and antibacterial agent. J. Asian Ceram. Soc. **2**, 357–365 (2014)

Reddy, K.H., Martha, S., Parida, K.M.: Fabrication of novel p-BiOI/n-ZnTiO$_3$ heterojunction for degradation of rhodamine 6G under visible light irradiation. Inorg. Chem. **52**, 6390–6401 (2013)

Regupathi, I., Vidya Shetty, K., Thanabalan, M.: Recent Advances in Chemical Engineering. Springer, Singapore (2016). https://doi.org/10.1007/978-981-10-1633-2

Roy, R., Agrawal, D., Cheng, J., Gedevanlshvili, S.: Full sintering of powdered-metal bodies in a microwave field. Nature **399**, 668–670 (1999)

Salavati-Niasari, M., Soofivand, F., Sobhani-Nasab, A., Shakouri-Arani, M., Yeganeh Faal, A., Bagheri, S.: Synthesis, characterization, and morphological control of ZnTiO$_3$ nanoparticles through sol-gel processes and its photocatalyst application. Adv. Powder Technol. **27**, 2066–2075 (2016)

Sedpho, S., Wongratanaphisan, D., Mangkorntong, P., Mangkorntong, N., Choopun, S.: Preparation and characterization of zinc titanate nanostructures by oxidation reaction technique. Nanotechnology **7**, 99–104 (2008)

Shukla, S.P., Gupta, G.S.: Toxic effects of omega chrome red ME and its treatment by adsorption. Ecotoxicol. Environ. Saf. **24**, 155–163 (1992)

Sing, K.S.W., Everett, D.H., Haul, R.A.W., Moscou, L., Pierotti, R.S., Rouquerol, J., Siemieniewska, T.: Reporting physisorption data for gas/solid systems with special reference to the determination of surface area and porosity. Pure Appl. Chem. **57**, 603–619 (1985)

Sirajudheen, P., Sanoop, K.B., Rashid, M.: Recent Advances in Chemical Engineering. 227–234 (2016). https://doi.org/10.1007/978-981-10-1633-2

Siwińska-Stefańska, K., Kubiak, A., Piasecki, A., Goscianska, J., Nowaczyk, G., Jurga, S., Jesionowski, T.: TiO$_2$-ZnO binary oxide systems: comprehensive characterization and tests of photocatalytic activity. Materials **11**, 841 (2018)

Slokar, Y.M., Le Marechal, A.M.: Methods of decoloration of textile wastewaters. Dyes Pigm. **37**, 335–356 (1998)

Surendar, T., Kumar, S., Shanker, V.: Influence of La-doping on phase transformation and photocatalytic properties of ZnTiO$_3$ nanoparticles synthesized via modified sol–gel method. Phys. Chem. Chem. Phys. **16**, 728–735 (2014)

Szczygielda, M., Prochaska, K.: Recovery of alpha-ketoglutaric acid from multi-component model solutions: impact of initial composition of diluate solution on the efficiency of the EDBM process. Desalin. Water Treat. **128**, 27–33 (2018). https://doi.org/10.5004/dwt.2018.22571

Tang, Y., Zhang, G., Liu, C., Luo, S., Xu, X.: Magnetic TiO$_2$-graphene composite asa high-performance and recyclable platform for efficient photocatalytic removal of herbicides from water. J. Hazard. Mater. **252–253**, 115–122 (2013)

Tian, H., Wang, S., Zhang, C., Veder, J.-P., Pan, J., Jaroniec, M., Wang, L., Liu, J.: Design and synthesis of porous ZnTiO$_3$/TiO$_2$

nanocages with heterojunctions for enhanced photocatalytic H$_2$ production. J. Mater. Chem. A. **5**, 11615–11622 (2017)

Tolba, G.M.K., Barakat, N.A.M., Bastaweesy, A.M., Ashour, E.A., Abdelmoez, W., El-Newehy, M.H., Al-Deyab, S.S., Kim, H.Y.: Hierarchical TiO$_2$/ZnO nanostructure as novel non-precious electrocatalyst for ethanol electrooxidation. J. Mater. Sci. Technol. **31**, 97–105 (2015)

Vlazan, P., Ursu, D.H., Irina-Moisescu, C., Miron, I., Sfirloaga, P., Rusu, E.: Structural and electrical properties of TiO$_2$/ZnO core–shell nanoparticles synthesized by hydrothermal method. Mater. Charact. **101**, 153–158 (2015)

Wang, H.Y., Yang, Y., Li, X., Li, L.J., Wang, C.: Preparation and characterization of porous TiO$_2$/ZnO composite nanofibers via electrospinning. Chin. Chem. Lett. **21**, 1119–1123 (2010)

Wang, C., Hwang, W., Chang, K., Ko, H., Hsi, C., Huang, H., Wang, M.: Formation and morphology of Zn$_2$Ti$_3$O$_8$ powders using hydrothermal process without dispersant agentor mineralizer. Int. J. Mol. Sci. **12**, 935–945 (2011)

Wang, Y., Fan, C., Wang, H., Wang, F., Xu, J., Duan, P., Zhang, Y.: Effects of TiO$_2$ on the sintering densification of UO$_2$–Gd$_2$O$_3$ burnable poison fuel. Ceram. Int. **41**, 10185–10191 (2015)

Wu, L., Wu, P., Zhu, Y., Zhu, N., Dang, Z.: Preparation and characterization of ZnTiO$_3$ TiO$_2$/pillared montmorillonite composite catalyst for enhanced photocatalytic activity. Res. Chem. Intermed. **42**, 5253–5268 (2016)

Xu, X., Wang, J., Tian, J., Wang, X., Dai, J., Liu, X.: Hydrothermal and post-heat treatments of TiO$_2$/ZnO composite powder and its photodegradation behavior on methyl orange. Ceram. Int. **37**, 2201–2206 (2011)

Yamaguchi, O., Morimi, M., Kawabata, H., Shimizu, K.: Formation and transformation of ZnTiO$_3$. J. Am. Ceram. Soc. **70**, C97–C98 (1987)

Yan, X., Zhao, C.L., Zhou, Y.L., Wu, Z.J., Yuan, J.M., Li, W.S.: Synthesis and characterization of ZnTiO$_3$ with high photocatalytic activity. Trans. Nonferrous Met. Soc. China **25**, 2272–2278 (2015)

Yang, L., Luo, S., Li, Y., Xiao, Y., Kang, Q., Cai, Q.: High efficient photocatalytic degradation of p-nitrophenol on a unique Cu$_2$O/TiO$_2$ p-n heterojunction network catalyst. Environ. Sci. Technol. **44**, 7641–7646 (2010)

Zaleska, A.: Doped-TiO$_2$: A Review. Recent Patents Eng. **2**, 157–164 (2008)

Zhang, J., Yan, S., Fu, L., Wang, F., Yuan, M., Luo, G., Xu, Q., Wang, X., Li, C.: Photocatalytic degradation of rhodamine B on anatase, rutile, and brookite TiO$_2$. J. Catal. **32**, 983–991 (2011)

Zhang, P., Shao, C., Zhang, M., Guo, Z., Mu, J., Zhang, Z., Zhang, X., Liu, Y.: Bi$_2$MoO$_6$ ultrathin nanosheets on ZnTiO$_3$ nanofibers: A 3D open hierarchical heterostructures synergistic system with enhanced visible-light-driven photocatalytic activity. J. Hazard. Mater. **217–218**, 422–428 (2012)

Zhang, Q., Zhang, K., Xu, D., Yang, G., Huang, H., Nie, F., Liu, C., Yang, S.: CuO nanostructures: synthesis, characterization, growth mechanisms, fundamental properties, and applications. Prog. Mater Sci. **60**, 208–237 (2014)

## Affiliations

**Adam Kubiak**[1] · **Katarzyna Siwińska-Ciesielczyk**[1] · **Zuzanna Bielan**[2] · **Anna Zielińska-Jurek**[2] · **Teofil Jesionowski**[1]

[1] Faculty of Chemical Technology, Institute of Chemical Technology and Engineering, Poznan University of Technology, Berdychowo 4, 60965 Poznan, Poland

[2] Department of Chemical Technology, Faculty of Chemistry, Gdansk University of Technology, Narutowicza 11/12, 80233 Gdansk, Poland